

www.acsaem.org Article

# Investigation of n-GaAs Photoanode Corrosion in Acidic Media with Various Thin Ir Cocatalyst Layers

Sahar Pishgar, Matthew C. Mulvehill, Saumya Gulati, Gamini U. Sumanasekera, and Joshua M. Spurgeon\*



Cite This: ACS Appl. Energy Mater. 2021, 4, 10799-10809



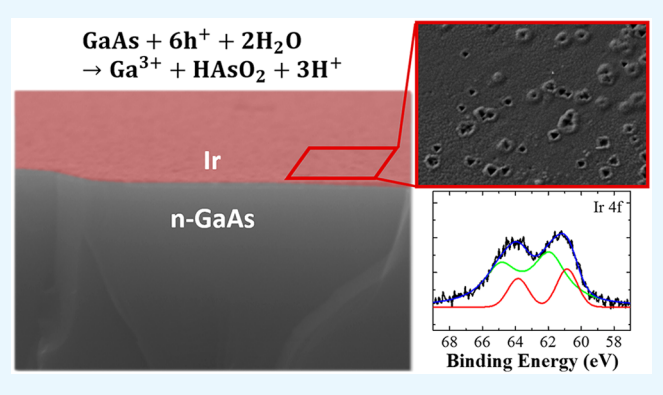
**ACCESS** 

Metrics & More

Article Recommendations

Supporting Information

ABSTRACT: n-GaAs is a well-developed III-V semiconductor with excellent light absorption and charge-transport properties, making it a promising candidate for an efficient photoanode. However, strong photocorrosion under anodic bias in aqueous electrolyte prohibits this semiconductor from having durable as well as efficient photoelectrochemical performance. In this work, the photocorrosion process of n-GaAs in acidic media was monitored via in situ UV-vis spectroscopic analysis of the dissolved elements in solution, with additional insight provided by SEM imaging and XPS surface analysis. A strong dependence of the current density vs potential behavior and associated photocorrosion was correlated to the n-type doping density, with the transition into degenerate-like behavior yielding distinctly different



photoelectrochemical and corrosion behavior. The photoanode behavior in acid was also investigated with thin surface layers of the acid-stable water oxidation catalyst Ir. Galvanic displacement was used to produce conformal thin films of Ir on n-GaAs, which was compared to films of Ir spin-coated from chemical precursors. In-situ UV—vis spectroscopy showed short-term decreases in the corrosion faradaic efficiency from the Ir films, but none provided sufficient protection to prevent GaAs photoetching from eventually becoming the dominant electrochemical pathway. The disparate nature of each Ir film is discussed to explain the observed differences in surface chemistry and morphology after photoanodic operation.

KEYWORDS: photoelectrochemistry, stability, GaAs, corrosion, water oxidation

#### 1. INTRODUCTION

Due to its widespread abundance, solar energy is one of the most promising clean alternatives to fossil fuels. Converting the energy of sunlight into the chemical bonds of clean fuels like hydrogen is an ideal route for the energy-dense storage of this intermittent resource. Direct photoelectrochemical (PEC) water-splitting has the potential to be a highly scalable and economic method to produce solar fuels. Tandem photoelectrodes of complementary bandgaps are one of the most efficient designs to achieve the requisite ~1.6 V of photovoltage to split water by running the hydrogen evolution reaction (HER) at the photocathode and oxygen evolution reaction (OER) at the photoanode. <sup>2,3</sup>

In striving to develop efficient and stable PEC systems, researchers have employed a variety of semiconductor types as photoelectrodes, including silicon, metal oxides, and III-Vs. 4-9 Metal oxides have demonstrated the greatest stability under water oxidation conditions, however, they typically exhibit large bandgaps and/or short minority-carrier diffusion lengths which have inhibited achieving high solar-to-hydrogen efficiency. <sup>10</sup> III-V semiconductors, in contrast, can cover a wide range of bandgaps, often have high charge-carrier

mobilities and diffusion lengths, and are among the best candidates for high efficiency photoelectrodes, especially as the top subcell material in a tandem cell design. <sup>3,9,11</sup> Although III—V semiconductors can enable systems of high solar-to-hydrogen efficiency, they generally suffer from corrosion in aqueous electrolytes under anodic conditions because the self-oxidation potentials of these materials are more negative than the water oxidation potential. <sup>12–14</sup> One strategy employed to mitigate photocorrosion of III—V photoelectrodes is to deposit a conformal thin film of a metal or metal oxide on the semiconductor surface as a protective barrier layer against chemical attack, which in some cases can also serve as an OER catalyst. <sup>14–19</sup>

Gallium arsenide (GaAs), one of the most well-developed III–V semiconductors, has played an important role in high-

Received: June 22, 2021 Accepted: September 30, 2021 Published: October 14, 2021





efficiency solar fuels systems, but it suffers from rapid photocorrosion resulting in the formation of an insulating oxide layer or dissolution of the photoelectrode. The stabilization of GaAs photoanodes through the deposition of a thin layer of a noble metal (e.g., Au, Pt, Rh) or a polymer such as polypyrrole has had only modest success, inhibiting the photocorrosion of n-GaAs for only a brief time. 20-24 Researchers have also studied the stability of GaAs photoanodes in conjunction with a surface monolayer of graphene, 16 which provided only limited protection in aqueous electrolyte. Greater stability on the order of hours was achieved for GaAs photoanodes in alkaline media using an in situ electrodeposited nickel-borate protective layer, although this required a p-n GaAs homojunction to maintain a high photovoltage. 1 Lastly, atomic layer deposition (ALD) of a conformal surface layer of TiO2 decorated with an OER catalyst has been widely reported for enhanced stabilization of III-V semiconductors such as GaAs and GaP. 8,14,17,25 The highest stability demonstrated to date has been for GaAs nanowire array photoanodes with a relatively thick (100 nm) ALD coating of amorphous TiO2 in combination with a Ni catalyst, which exhibited continuous solar-driven water oxidation in alkaline media for over 600 h with only modest current decay.<sup>25</sup> The success of this method relies on thick ALD layers to achieve near-total suppression of pinholes and failure points, which in turn depends upon an amorphous TiO2 phase with defects providing a band of intergap states for efficient hole charge-transfer across the interface. <sup>17</sup> However, the replication of this precise layer has proven difficult for many laboratories.

To improve the practicality of III-V semiconductor photoanodes, a detailed understanding of the photocorrosion process is needed along with simple, cost-effective corrosion protection strategies. Researchers have studied the mechanism of GaAs photocorrosion and proposed reaction pathways that explain the different dissolution behavior of the Ga and As components in acidic vs alkaline media, as well as the formation of oxide layers on n-GaAs electrodes in neutral electrolyte. 26-29 Herein, the focus is on n-GaAs photoanodic behavior in aqueous acidic electrolyte, similar to the operating media for some of the most advanced electrolyzers. Ideally, the semiconductor surface would be conformally coated in a lowcost process with a thin layer of chemically inert material which simultaneously enhances the OER kinetics. Electroless deposition via galvanic displacement of metals onto a semiconductor surface is a simple, cost-effective, highthroughput method for thin layers that has routinely been employed to produce metal-semiconductor contacts. Reports of galvanic displacement of noble metals on n-GaAs have shown the formation of thin films of Au, Ag, and Pt. 30-32 The promise of this method for conformal surface coverage is highlighted by a recent report using electroless deposition of gold on amorphous-TiO2 protected p+-GaAs electrodes as a failure detection method for the protection layer by imaging Au deposits in the pinholes.<sup>33</sup> However, Ir oxide is one of the only highly active OER catalysts which is stable under anodic potentials in strongly acidic media.<sup>34</sup> According to the reduction potentials of different noble metal anions with respect to the valence band of GaAs, Ir can be deposited from hexachloroiridate salts onto n-GaAs by galvanic displacement. 21,35 The investigation of the photoanodic behavior and corrosion-inhibiting properties of electrolessly deposited Ir on n-GaAs is therefore of interest.

Herein, we have investigated the GaAs photocorrosion process in acidic media, with proposed insights on the differences observed depending on the n-type doping density. Photocorrosion of electrodes has been studied via in situ UVvis spectroscopy to quantify the faradaic efficiency for GaAs dissolution and supplemented by SEM and X-ray photoelectron spectroscopy (XPS), following our previous work.<sup>36</sup> The effect on the photocorrosion process of thin Ir surface layers, deposited by either galvanic displacement or spincoated from one of two Ir precursors, was investigated as well. The limitations of these optically thin layers of Ir to protect GaAs photoanodes are described through electrochemical measurements and morphological and chemical characterization of the interface. The work demonstrates how the inexpensive, novel in situ UV-vis spectroscopy method can enable active monitoring and quantification of the corrosion reaction faradaic efficiency, permitting researchers to diagnose the extent of electrochemical protection afforded by a surface treatment such as the contiguous, oxidatively acid-stable Ir films employed in this study. Moreover, notable differences in the observed corrosion faradaic efficiency can highlight for researchers when a distinct change in material degradation behavior has occurred, such as that observed herein for different GaAs doping densities at the same applied bias. An increased understanding of the GaAs photocorrosion process as well as the effects of the catalyst layer preparation method and corresponding failures in the protective layer can ultimately help researchers navigate the path to develop stable and efficient III-V photoanodes.

#### 2. EXPERIMENTAL SECTION

**2.1. Electrode Fabrication.** n-GaAs wafers ((111), Si-doped to  $1-5\times 10^{18}~{\rm cm}^{-3}$ , Precision Micro-Optics) were used as the working electrodes in all experiments unless stated otherwise. One other commercial source of comparable n-GaAs wafers ((111B), Si-doped to  $2.2-2.8\times 10^{17}~{\rm cm}^{-3}$ , University Wafer, Inc.) was tested for its photoelectrochemical performance, as shown in Figure 1a. Ohmic contacts were made to the working electrodes by lightly scratching Ga/In eutectic onto the back of the wafer followed by attaching copper tape as a current collector.

Some of the electrodes were further decorated with Ir or IrO<sub>x</sub> oxygen evolution reaction cocatalyst. A thin layer of electrolessly deposited iridium (hereafter referred to as Ir(el)) was produced via a galvanic displacement method to deposit iridium catalyst on n-GaAs substrates. The n-GaAs was pretreated by immersion in 3 M HCl for 3 min and then thoroughly rinsed with 18 M $\Omega$ -cm water. GaAs samples were subsequently immersed in a solution of 1 mM hydrogen hexachloroiridate(IV) hydrate, H<sub>2</sub>IrCl<sub>6</sub>·xH<sub>2</sub>O (99%, Alfa Aesar), in 1 M H<sub>2</sub>SO<sub>4</sub> for 24 h followed by a thorough rinse. In some other samples, IrOx was deposited by a spin-coating method using one of two different iridium precursors. In one case, a solution of 40 mM iridium(III) chloride, IrCl<sub>3</sub> (99.8%, Alfa Aesar), in isopropanol was used to make a thin Ir layer (hereafter referred to as Ir(ch)). In the second case, a solution of 40 mM iridium(III) acetylacetonate, Ir(acac)<sub>3</sub> (98%, Strem Chemicals, Inc.), in chloroform was used to make the thin Ir layer (hereafter referred to as Ir(ac)). In both cases, 40  $\mu$ L of solution was applied while the substrate was rotating at 200 rpm, then the substrate rotation rate was increased to 2000 rpm and spun for 60 s. The substrates were then heated at 60 °C for 5 min to evaporate any residual solvent before annealing them in a preheated furnace at 250 °C for 2 h under ambient air. <sup>18</sup> A Zygo noncontact 3D optical profilometer was used to measure the thickness of Ir thin films.

**2.2. Photoelectrochemical Measurements.** Photoelectrochemical measurements were conducted in a quartz cuvette simultaneously with UV—vis spectroscopy of the electrolyte for in situ photocorrosion detection as reported in our previous work.<sup>36</sup> Briefly, a 5

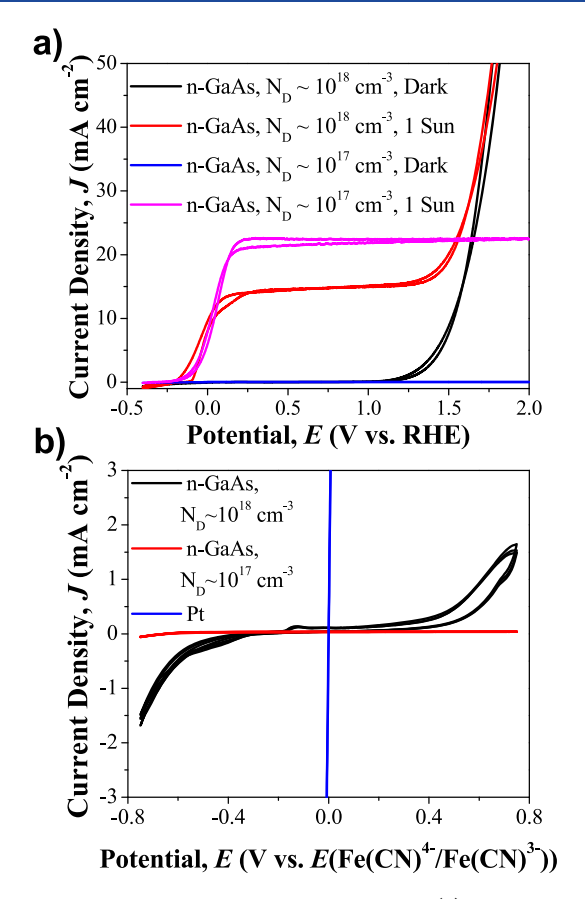


**Figure 1.** Bare n-GaAs electrochemical behavior. (a) Current density vs potential (J-E) in 1 M  $\rm H_2SO_4$  in the dark and under 1 Sun AM1.5 illumination for GaAs wafers of two different doping densities. (b) Current density vs potential (J-E) behavior in 0.5 M  $\rm K_4Fe(CN)_6-0.05$  M  $\rm K_3Fe(CN)_6(aq)$  in the dark for (black line) n-GaAs of  $N_{\rm D}\approx 10^{18}$  cm<sup>-3</sup>, (red line) n-GaAs of  $N_{\rm D}\approx 10^{17}$  cm<sup>-3</sup>, and (blue line) a Pt electrode.

mm diameter hole was drilled on one vertical face of the cuvette for electrolyte contact with the n-GaAs working electrode. The n-GaAs was pressed against the outside of the cell at the drilled hole using a thin Teflon gasket to prevent electrolyte leakage. The 1.0 M H<sub>2</sub>SO<sub>4</sub> electrolyte volume was kept low (1.25 mL) to promote a higher concentration of dissolved electrode species to maximize the UV-vis detection sensitivity. A 1 mm diameter leak-free micro Ag/AgCl (Innovative Instruments, Inc.) was used as the reference electrode. The Pt mesh counter electrode was confined to a secondary small container connected to the cuvette electrolyte through a 2 mm diameter bridging tube with a glass frit (KZT-2 tube, Innovative Instruments, Inc.). The counter electrode was separated from the main cell to avoid Pt contamination of the working electrode, to prevent any back reactions of the dissolved semiconductor species at the counter, and to keep hydrogen bubbles generated at the counter from obscuring the illumination pathway. Illumination consisted of 1-Sun AM1.5 white light (300 W Xe lamp, Newport 6258 with AM1.5 global filter) directed through the electrolyte normal to the working electrode and orthogonal to the UV-vis input beam passed through the electrolyte parallel to the working electrode surface. A Si photodiode (Thorlabs, FDS100-CAL) was used to calibrate the intensity of the simulated sunlight. All electrochemical measurements were performed using an Autolab PGSTAT 100N (Metrohm) potentiostat. The results are reported versus the reversible hydrogen electrode (RHE) scale according to  $V_{
m RHE}$  =  $V_{
m Ag/AgCl}$  + 0.197 + 0.059pH, where the electrolyte pH was 0.

**2.3.** Characterization Methods. In-situ UV—vis spectroscopy measurements were performed with an Agilent Cary 60 spectrophotometer in background correction mode with 1.0 M H<sub>2</sub>SO<sub>4</sub> as the

background. Absorbance data was calibrated to dissolved Ga and As concentrations using inductively coupled plasma mass spectrometry (ICP-MS, Agilent 7900). Separate calibration curves were measured for GaAs at 1.0 and 1.5 V vs RHE (Figure S3 of the Supporting Information, SI). The dissolved Ga concentration was used to calculate the estimated faradaic efficiency of the GaAs corrosion reaction by determining the charge required to oxidize GaAs to produce the observed quantity of dissolved Ga (assuming 6 e<sup>-</sup> per molecule of GaAs) and dividing this by the total charge passed during the potentiostatic measurement at the time of the absorbance measurement.

The electrode surfaces were imaged with scanning electron microscopy (SEM) using a NOVA FEI microscope or Thermo-Fisher Scientific Apreo C LoVac FESEM at an accelerating voltage of 20 kV. Surface elemental analysis was conducted using X-ray photoelectron spectroscopy (XPS) with a VG Scientific Multilab 3000 custom-built ultrahigh vacuum (UHV) system with Al–K $\alpha$  radiation. XPSPEAK 4.1 software was used for peak deconvolution and the XPS data analysis.

# 3. RESULTS AND DISCUSSION

3.1. Bare n-GaAs Photocorrosion Behavior. Photoanodes of (111)-oriented GaAs doped n-type with Si donors were used throughout the experiments. The majority of samples available for study were doped to  $N_{\rm D} \approx 10^{18}~{\rm cm}^{-3}$ . The measured dark and 1-Sun photoelectrochemical energy conversion behavior of bare n-GaAs photoanodes in 1 M H<sub>2</sub>SO<sub>4</sub> is shown in Figure 1a. These photoanodes had an onset potential under illumination of  $-0.24~\mathrm{V}$  vs RHE and a lightlimited current density of 12-14 mA cm<sup>-2</sup>. A typical highquality GaAs photoactive layer has a photovoltage of ~1 V or less, which is not sufficient to split water on its own. Thus, the photocurrent at voltages negative of 0 V vs RHE is primarily indicative of electrochemical GaAs photocorrosion. Notably, the oxidative current increased exponentially at potentials >1.2 V vs RHE. The exponential increase at more anodic potentials was similarly observed in the dark and can be attributed to electrocatalytic Butler-Volmer kinetics. Again, the onset of this behavior in the dark at potentials less than the oxygen evolution reaction potential (OER at 1.23 V vs RHE) indicates that the charge passed is contributing to semiconductor corrosion rather than water oxidation. Cycling the potential to values beyond 1.5 V vs RHE led to high anodic currents, rapid and visible pitting and etching of the semiconductor surface, and corresponding irreversible decreases in the light-limited current density with successive voltage scans (Figure S1).

In an ideal semiconductor-liquid photoelectrochemical junction for a photoanode, increasing anodic potential puts the diode into reverse bias which leads to stronger band bending in the depletion region. The resulting energy barrier across the depletion region inhibits majority-carrier transfer from the semiconductor bulk, leading to one-way charge flow and a flat current profile which prevents the type of exponential current increase exhibited by the n-GaAs ( $N_{\rm D}\approx 10^{18}~{\rm cm}^{-3}$ ) anodes in the dark. Indeed, some samples of similar n-GaAs at a lower doping ( $N_{\rm D}\approx 10^{17}~{\rm cm}^{-3}$ ) from a different commercial source were obtained and measured for comparison. As shown in Figure 1a, these photoanodes exhibited higher light-limited current density ( $\sim$ 22 mA cm $^{-2}$ ) and did not display the Butler–Volmer-type exponential current increase in the dark or under illumination at higher potentials.

The observed energy-conversion behavior for the more highly doped n-GaAs electrodes of a photodiode response conflated with dark electrocatalytic Butler—Volmer kinetics has frequently been reported for metal oxide photoanodes,

especially in the presence of a cocatalyst. In some of those cases, the exponential current increase at higher potentials was attributed to shunt pathways for charge-transfer across the electrode interface to bypass the reverse bias energy barrier, thus allowing dark electrocatalytic behavior to occur in parallel with the illuminated photodiode behavior.<sup>37</sup> This possibility was tested for the n-GaAs photoanodes in this work using the kinetically fast one-electron redox couple ferro-/ferricyanide. As shown in Figure 1b, the lower doped n-GaAs electrodes appeared highly resistive in the ferro-/ferricyanide solution, due to the band bending produced by the difference between the redox couple potential and the semiconductor Fermi level. A metallic Pt electrode, in contrast, exhibited highly ohmic behavior with low resistance. If the dark Butler-Volmer exponential response in the higher doped GaAs anodes was attributable to parallel shunt pathways for charge flow, then a similar low-resistance ohmic response would be expected.<sup>37</sup> However, the  $N_{\rm D} \approx 10^{18}~{\rm cm}^{-3}$  doped n-GaAs electrodes did not exhibit ohmic behavior but instead showed rectifying behavior less resistive than the  $N_{\rm D} \approx 10^{17}~{\rm cm}^{-3}$  doped n-GaAs. The exponential increase in dark anodic current for the higher doped GaAs was therefore not attributed to shunt pathways for charge-carriers to bypass the band bending.

The electrochemical energy-conversion behavior exhibited by the higher doped n-GaAs is instead consistent with the onset of degenerate-like semiconductor properties. This finding is supported by literature reports that the low effective mass of electrons in GaAs leads to degenerate properties at a relatively low n-type doping of  $5 \times 10^{17} - 1 \times 10^{18}$  cm<sup>-3</sup>. Strongly degenerate semiconductors are so highly doped that the excess majority carriers and sharply bent bands lead to metallic characteristics and photoinactive properties. The decreased light-limited photocurrent for the  $N_{\rm D} \approx 10^{18}~{\rm cm}^{-3}$ doped n-GaAs relative to the  $N_{\rm D} \approx 10^{17}~{\rm cm}^{-3}$  doped n-GaAs is consistent with the onset of degeneracy as charge-carriers can increasingly tunnel through the sharply bent bands in a narrower depletion region which also decreases the depth for charge-carrier separation driven by migration in the electric field. This interpretation is further in agreement with past reports of increased anodic dark current for GaAs with increasing N<sub>D</sub> owing to electrons tunnelling a barrier which becomes thinner with doping density.<sup>26,39,40</sup> Specifically, Allongue et al. proposed a GaAs corrosion mechanism in which Ga and As surface atoms that are partially bonded to the lattice and to species of the solution give rise to interface states within the GaAs bandgap, and injection of electrons from these states into the GaAs bulk leads to oxidative corrosion by holes at that site.<sup>26</sup> Thus, the exponential increase of corrosion current for higher doped n-GaAs beyond 1.2 V vs RHE (Figure 1a) could reasonably be interpreted as electrons from these interface states increasingly tunnelling through the narrow energy barrier of a quasi-degenerate semiconductor resulting in rapidly increasing surface corrosion with increased anodic bias. Figure 2 illustrates the difference in the proposed band bending schemes between the  $N_{\rm D} \approx 10^{17}$  and  $10^{18}$  cm<sup>-3</sup> cases.

The bare n-GaAs photoanodes were measured under 1 Sun AM1.5 illumination at potentiostatic conditions in a quartz cuvette reactor cell with simultaneous in situ UV-vis spectroscopic analysis of the electrolyte, as reported in our previous work.<sup>36</sup> Control measurements and ICP-MS calibration data for the in situ UV-vis spectroscopy for GaAs are reported in Figures S2 and S3, respectively. Figure 3a shows the corresponding current density vs time curves for the

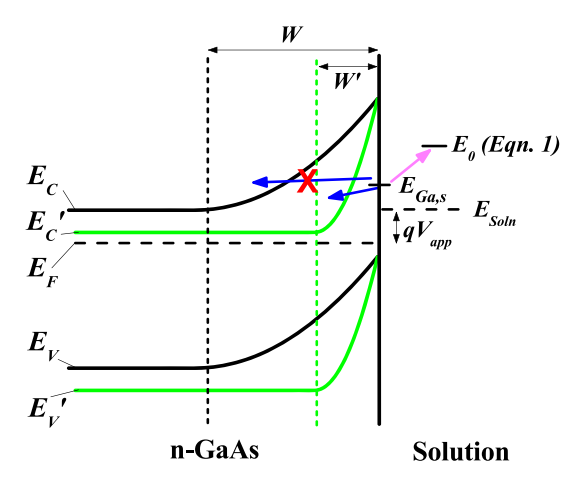


**Figure 2.** Band diagram for the proposed scheme of doping density dependence on the photoelectrochemical behavior for GaAs photocorrosion. Conduction  $(E_{\rm C})$  and valence  $(E_{\rm V})$  bands are black for the nondegenerate case and green for the case transitioning to degeneracy  $(E_{\rm C}'$  and  $E_{\rm V}')$ . The junction is shown in reverse bias with applied voltage,  $V_{\rm app}$ , and depletion width, W.  $E_{\rm Ga,S}$  represents the energy level for Ga-sites at the surface, and  $E_0$  is the energy for the corrosion half-reaction GaAs + 3h $^+$   $\rightarrow$  Ga $^{3+}$  + As $^0$ . Arrows show the direction of electron transfer (blue) and hole transfer (pink).

n-GaAs at 1.0 and 1.5 V vs RHE. The oscillations in these curves were observed to correspond to bubble formation and release from the exposed wafer in the 5 mm diameter hole in the cuvette. By comparing the detected concentration of dissolved Ga ions to the charge passed over the same time period, the faradaic efficiency for the GaAs corrosion reaction was plotted over the course of a 60 min measurement (Figure 3b). This calculation assumed that six holes are required to dissolve each molecule of GaAs. Although literature reports vary on the resulting byproducts and the species state of the dissolved As upon GaAs oxidative corrosion in acidic media, a value of n = 6 for the required number of charges passed per GaAs has been consistently identified. The overall corrosion reaction in acid is proposed to follow a two-step process in which Ga is selectively etched first, leaving behind As<sup>0</sup> metal which is subsequently electrochemically oxidized and dissolved:

$$GaAs + 3h^{+} \rightarrow Ga^{3+} + As^{0}$$
 (1)

$$As^{0} + 3h^{+} + 2H_{2}O \rightarrow HAsO_{2} + 3H^{+}$$
 (2)

$$GaAs + 6h^{+} + 2H_{2}O \rightarrow Ga^{3+} + HAsO_{2} + 3H^{+}$$
 (3)

Using the overall reaction in eq 3, the faradaic efficiency for GaAs corrosion was determined to be >95% at 1.0 V vs RHE (Figure 3b). This result is an indication that six holes per GaAs molecule is accurate under these conditions and that the semiconductor oxidative corrosion reaction is strongly kinetically favored at this potential relative to the oxygen evolution reaction, which would reduce the faradaic efficiency for GaAs dissolution.

Interestingly, at the higher current density under 1.5 V vs RHE for  $N_{\rm D}\approx 10^{18}~{\rm cm}^{-3}$ , the calculated faradaic efficiency for GaAs corrosion was 115–122% (Figure 3b). This result is in sharp contrast to the measured GaAs corrosion faradaic efficiency at the same potential for a photoanode of  $N_{\rm D}\approx 10^{17}~{\rm cm}^{-3}$ , which was measured between 75–90%. Clearly, greater than 100% faradaic efficiency is not possible, and this is an

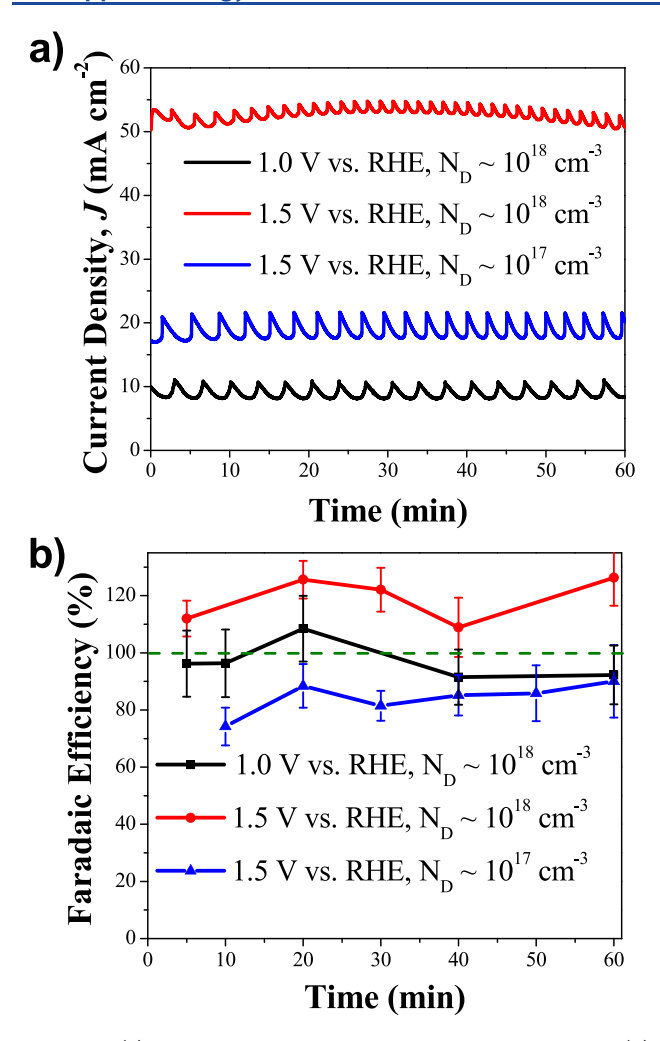


**Figure 3.** (a) Illuminated chronoamperometric behavior and (b) corresponding faradaic efficiency for the corrosion reaction for n-GaAs in the UV-vis cuvette reactor. The FE was determined assuming six electrons (n = 6) per detected Ga atom.

indication that the assumption of six holes per molecule of dissolved GaAs did not hold at this condition for the higher doping. While no macroscopic particles or precipitates were observed in the electrolyte, there is a possibility that under the rapid etching conditions at 1.5 V vs RHE some unreacted microparticulates of GaAs may be released from the surface and quantified by ICP–MS, leading to a higher detected

concentration of Ga ions than could be attributed to the electrochemical dissolution alone. SEM images of the GaAs surface after extended operation at these potentials highlight the feasibility of this explanation (Figure 4). While operation at 1.0 V vs RHE led to micron-scale etch pits and pock marks across the surface, operation at 1.5 V vs RHE led to deep etching with some much larger pits and valleys as well as flaky material and particles at the surface (Figure S4), which if released into the electrolyte would lead to higher elemental concentrations detected by ICP-MS and correspondingly higher calculated faradaic efficiency values. It is also possible that the mechanism for corrosion at 1.5 V vs RHE on the  $N_{\rm D} \approx$ 10<sup>18</sup> cm<sup>-3</sup> doped n-GaAs, in which significant current can pass in the dark as theorized above via electron tunnelling of the band bending, is distinctly different from the corrosion route at a light-limited current density dominated by the transfer of photogenerated holes from the valence band to the corroding surface sites. A competing corrosion reaction requiring less than six holes per GaAs could thus alternatively account for the observed faradaic efficiency at 1.5 V vs RHE for  $N_{\rm D} \approx 10^{18}$ cm<sup>-3</sup>, though such a route is speculative at this stage.

One other possible explanation considered was that the reactions of eqs 1-3 might remain the dominant pathway for the electrochemical corrosion, but the significantly increased current density observed at 1.5 V vs RHE for  $N_{\rm D} \approx 10^{18}~{\rm cm}^{-3}$ could conceivably lead to kinetic constraints causing an imbalance in the rates of the reactions in eqs 1 and 2. In this case with preferential electrochemical etching of the Ga site,<sup>26</sup> the excess As<sup>0</sup> would need to be chemically dissolved to maintain the ~1:1 Ga:As ratio for dissolved atoms that was measured by ICP-MS (Figure S3). However, it has been reported that under strongly acidic conditions, chemical etching of GaAs preferentially etches Ga sites leaving an Asrich surface. 26 This finding has been confirmed with XPS using a UHV chamber coupled with the electrochemical cell to enable surface analysis before ambient oxidation of the elemental As<sup>0</sup> layer. <sup>42,43</sup> The As<sup>0</sup> layer is thus considered thermodynamically stable at pH 0,26 making the chemical dissolution of this layer an unlikely explanation for the calculated >100% faradaic efficiency observed at 1.5 V vs RHE. We thus attribute this result to one or both of the previous two explanations.

Surface analysis of the bare n-GaAs by XPS after operation at 1.0 and 1.5 V vs RHE are reported in Figure 5. For pristine samples, the Ga 2p and As 3d peaks were dominated by the GaAs phase with only a minor shoulder peak attributed to the

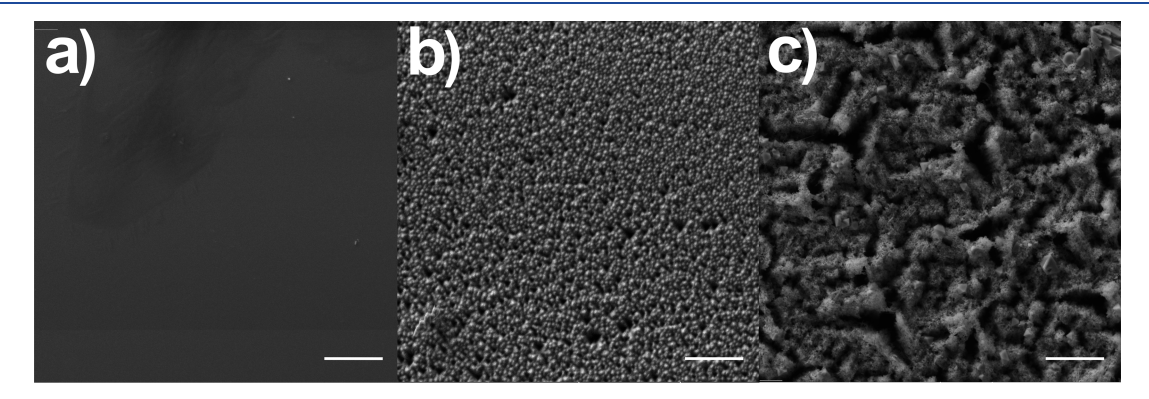
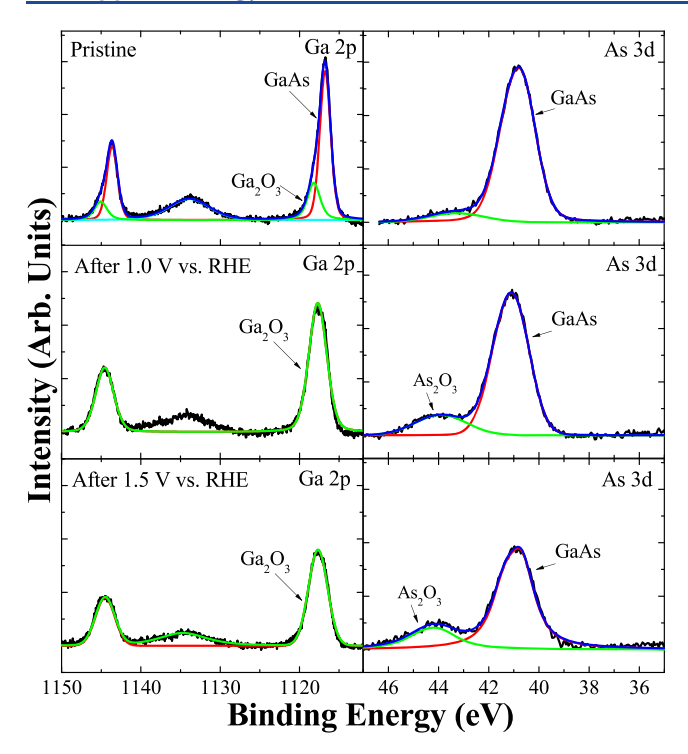


Figure 4. SEM images for bare n-GaAs ( $N_{\rm D}\approx 10^{18}~{\rm cm^{-3}}$ ) photoanodes (a) pristine, (b) after 2 h under 1 Sun at 1.0 V vs RHE, and (c) after 2 h under 1 Sun at 1.5 V vs RHE. Scale bar is 20  $\mu$ m in all panels.



**Figure 5.** XPS spectra of bare n-GaAs  $(N_D \approx 10^{18}~\text{cm}^{-3})$  photoanodes. Samples are (top) pristine, and after 2 h at 1 Sun in 1 M H<sub>2</sub>SO<sub>4</sub> at either (middle) 1.0 V vs RHE or (bottom) 1.5 V vs RHE.

native surface oxide phases  $Ga_2O_3$  and  $As_2O_3$ . Following oxidative corrosion in aqueous acid and exposure to air, the Ga 2p peak position shifted and was primarily assigned to  $Ga_2O_3$ . For the As 3d peaks, a significantly stronger  $As_2O_3$  shoulder peak developed which was most intense relative to the GaAs peak for the 1.5 V vs RHE condition. Elemental  $As^0$  As 3d peaks occur within 0.5 eV of the GaAs peak binding energy and were not readily resolved in the measured spectra. <sup>44,45</sup> Given the highly porous nature of the  $As^0$  layer formed during acidic etching observed here (Figure 4) and reported elsewhere, <sup>29</sup> it is not surprising that this layer was primarily converted to  $As_2O_3$  after exposure to air.

3.2. Thin Layer Ir-Coated n-GaAs Photocorrosion Behavior. One strategy that has had success at limiting the photocorrosion of n-GaAs in aqueous media is to use chalcogenide redox couples, which provide stabilization by being kinetically easier to oxidize than the semiconductor itself. However, to use this material as a water-splitting photoanode, the holes should be directed to the oxygen evolution reaction (OER). The decoration of a photoanode with a low OER overpotential cocatalyst has been shown to improve the OER kinetics enough to promote water oxidation to the dominant reaction pathway in other acidic systems.<sup>3</sup> The GaAs self-oxidation potential is thermodynamically negative of the OER potential, however, so OER kinetic improvements alone are not predicted to stabilize the GaAs surface. 12 To prevent oxidative corrosion while still maintaining photoelectrochemical water oxidation, the Ga and As sites should be physically protected from reaction with the acidic aqueous media with a thermodynamically stable layer. This approach was the premise for studying n-GaAs photocorrosion with thin layers of the acid-stable OER catalyst IrO<sub>x</sub>. While a thick layer is more likely to provide robust coverage and

protection, it would also absorb more light and detrimentally affect the band bending at the photoelectrochemical junction (Figures S6 and S7).

Three methods of thin-layer Ir application were tested as described above: electroless deposition (Ir(el)), spin-coated IrCl<sub>3</sub> (Ir(ch)), and spin-coated Ir(acac)<sub>3</sub> (Ir(ac)). The uniform formation of an Ir layer through the electroless method was confirmed via SEM and EDS mapping (Figure S5). Thicknesses of the Ir layers were estimated by profilometry and estimated to be 25–30 nm for Ir(el), 4–8 nm for Ir(ch), and 8–12 nm for Ir(ac). Representative examples showing the Ir/n-GaAs *J–E* curves are shown in Figure 6a. The effect of the

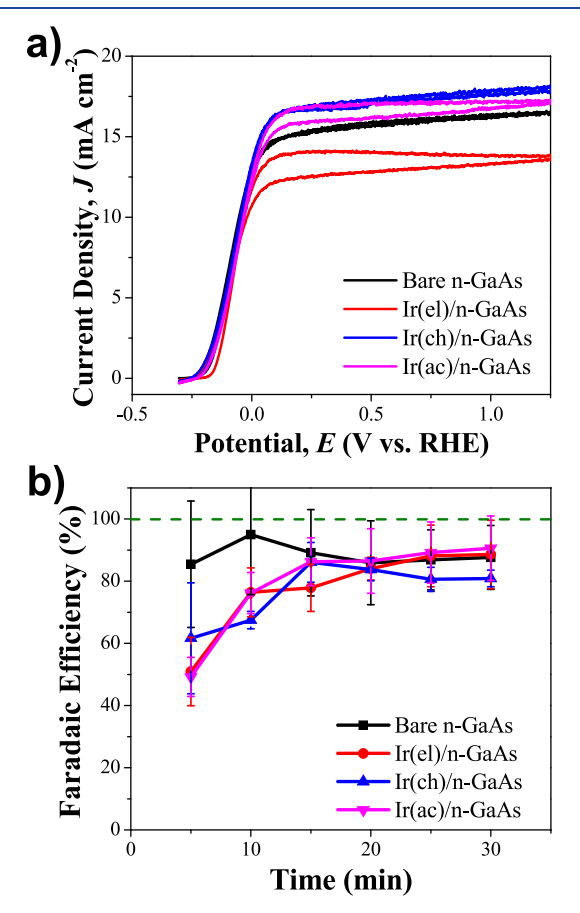


**Figure 6.** (a) Current density vs potential behavior for bare n-GaAs and Ir-coated n-GaAs prepared by electroless iridium deposition (Ir(el)), spin-coating iridium chloride (Ir(ch)), or spin-coating iridium acetylacetonate (Ir(ac)), under 1 Sun in 1 M  $\rm H_2SO_4$ . (b) Faradaic efficiency for GaAs photocorrosion as measured by in situ UV—vis spectroscopy on bare n-GaAs and Ir-coated n-GaAs electrodes. All photoanodes had  $N_{\rm D}\approx 10^{18}~\rm cm^{-3}$ . Error bars represent the deviation over three duplicate measurements.

thin Ir layer on the n-GaAs current density vs potential behavior in each case was minimal, though a modest current density decrease was observed for electroless Ir. The potential range of operation for these electrodes was intentionally maintained below 1.5 V vs RHE to avoid the rapid etching observed at more anodic potentials. Thicker Ir layers were avoided to prevent decreased photoelectrochemical energy-conversion behavior. Transmittance data for the spin-coated Ir layers as a function of thickness are shown in Figure S6. Also, photoelectrochemical current density vs potential data for thicker Ir layers on n-GaAs are provided in Figure S7, which

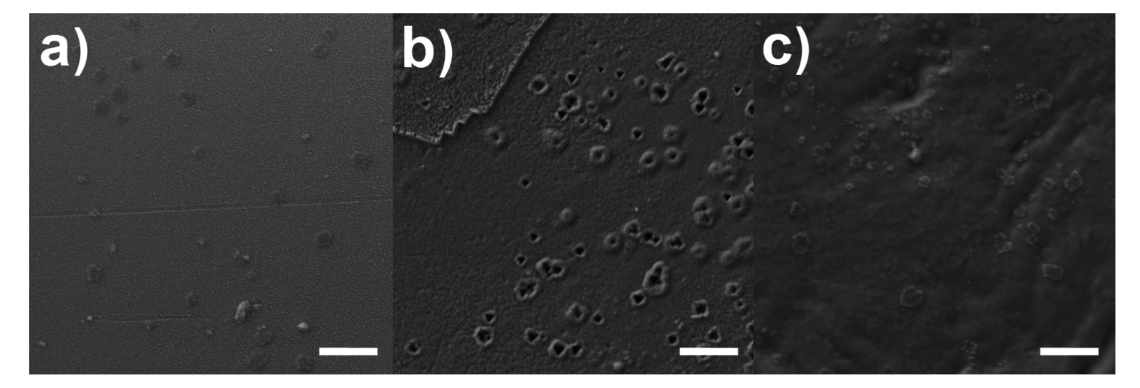


Figure 7. SEM images for Ir-coated GaAs ( $N_{\rm D}\approx 10^{18}~{\rm cm^{-3}}$ ) after 10 min at 1.0 V vs RHE at 1 Sun for (a) Ir(el), (b) Ir(ch), and (c) Ir(ac). Scale bar is 20  $\mu$ m in all panels.

displays a decrease in light-limited current density for thicker layers due to parasitic absorption in the catalyst as well as poorer junction properties as thicker Ir at the GaAs interface degrades the rectifying behavior of the liquid junction. For the thin Ir coatings, the time-dependent faradaic efficiency of the GaAs corrosion reaction was monitored at the light-limited current density at 1.0 V vs RHE using in situ UV—vis spectroscopy (Figure 6b). Unfortunately, none of the thin cocatalyst surface layers had a dramatic effect on the corrosion faradaic efficiency profile, with each Ir/n-GaAs photoanode reaching comparable behavior to a bare n-GaAs after 15—20 min. Before 15 min a modest decrease in the corrosion faradaic efficiency was detected for all three Ir deposition approaches, though it was not measured less than ~50%.

Materials characterization of the Ir/n-GaAs samples after operation in acid provides some additional insights on the physical differences between the electrodes by the method of Ir deposition. Figure 7 shows SEM images of the electrode surfaces after 10 min at 1.0 V vs RHE, long enough for corrosion to cause morphological changes but during the critical early stage when some effect on the faradaic efficiency was still detectable. The Ir(el)/n-GaAs sample after 10 min showed only the small beginnings of etch pits with fairly uniform distribution. After 2 h of photoetching, these sites grew into deeper triangular pits approximately 5  $\mu$ m across which fully covered the surface of the exposed area (Figure S8). The Ir(ch)/n-GaAs electrode, in contrast, displayed sizable 3-5  $\mu$ m triangular etch pits even after only 10 min, although these etch pits were much less dense and nonuniformly distributed (Figure 7b). Moreover, for these etch pits, the SEM images show the rougher Ir(ch) surface layer was disturbed near the edge of the triangular pits, in some cases appearing to spill over into the pit. This morphology is consistent with corrosion proceeding through pinholes in the Ir(ch) layer, leading to faster etching through the limited pinhole area and creating larger pits which start to undercut the Ir(ch) layer beside the pinhole. In some cases, flaking and lift-off of the Ir(ch) compact surface layer was observed in the vicinity of an etch pit (Figure S9). The uniform, slower growing etch pits on the Ir(el)/n-GaAs indicate etching occurring across the entire surface area rather than via isolated pinholes. The mechanism for preferential formation of triangular etch pits on these surfaces is likely similar to the process we described previously for n-GaP in acid.36 Photogenerated minority-carrier holes from the valence band are most likely to populate surface states within the band gap, leading to accelerated oxidative corrosion at interface defects

which become nucleation sites for etch pits. Because of the different energy density required to break the bonds in different crystal orientations, anisotropic etching can occur. The (111) Ga-terminated surface in particular has the fastest kinetics for surface corrosion in acid, and this selective etching leads to pyramidal etch pits on the GaAs(111) wafers used in this work. Interestingly, for the Ir(ac)/n-GaAs no obvious etch pits were observed, but the surface layer, which appeared less compact and more fluid in its morphology than the other electrode types, did develop noticeable contours which were not present in the flat pristine sample. We speculate that the electrolyte may permeate this less compact IrO<sub>x</sub> layer and lead to corrosion underneath areas of the film.

Surface analysis of the Ir/n-GaAs also indicates notable differences between electrode interfaces that may affect the corrosion process. XPS spectra for the Ga 2p, As 3d, and Ir 4f regions are plotted in Figure 8 for the three types of Ir-coated n-GaAs photoanodes before and after operation at 1.0 V vs RHE. For each photoanode type, the pristine and used samples were measured at the same time and their relative intensities are plotted on the same scale for each binding energy region, so the before and after data can be directly compared. For the Ir(el)/n-GaAs photoanode, the significantly higher intensity of the As 3d peak for As<sub>2</sub>O<sub>3</sub> relative to the peak for GaAs distinguishes this electrode type from the bare n-GaAs and the other Ir-coated photoanodes. Importantly, the enhancement of the As<sub>2</sub>O<sub>3</sub> peak is present even on the pristine Ir(el)/n-GaAs before photoelectrochemical operation. The prevalence of As<sub>2</sub>O<sub>3</sub> at the surface is attributable to the mechanism of electroless iridium deposition via galvanic displacement. In a galvanic displacement reaction, a noble metal ion in solution can be reduced to its metal form and replace the surface layer of a substrate if the noble metal/metal ion redox couple has a standard electrochemical potential greater than that of the substrate metal/metal ion potential. If the material and pH conditions allow a stable substrate oxide, then the noble metal deposition may coincide with surface oxidation as well.<sup>35</sup> In this case, the hexachloroiridate ion/iridium redox standard potential is positive of the GaAs valence band as well as the GaAs corrosion potentials.<sup>21</sup> Metal deposition on the semiconductor surface occurs via local anode and cathode sites, in which electrons from the valence band reduce the IrCl<sub>6</sub><sup>2-</sup> to plate Ir<sup>0</sup> on the surface at a cathode site while a local anode site undergoes GaAs oxidation resulting in an As<sub>2</sub>O<sub>3</sub>-rich surface. With co-located anode and cathode sites, metal deposits produced by galvanic displacement are usually porous. 48 Thus, acidic electrolyte contact with the semiconductor surface

www.acsaem.org

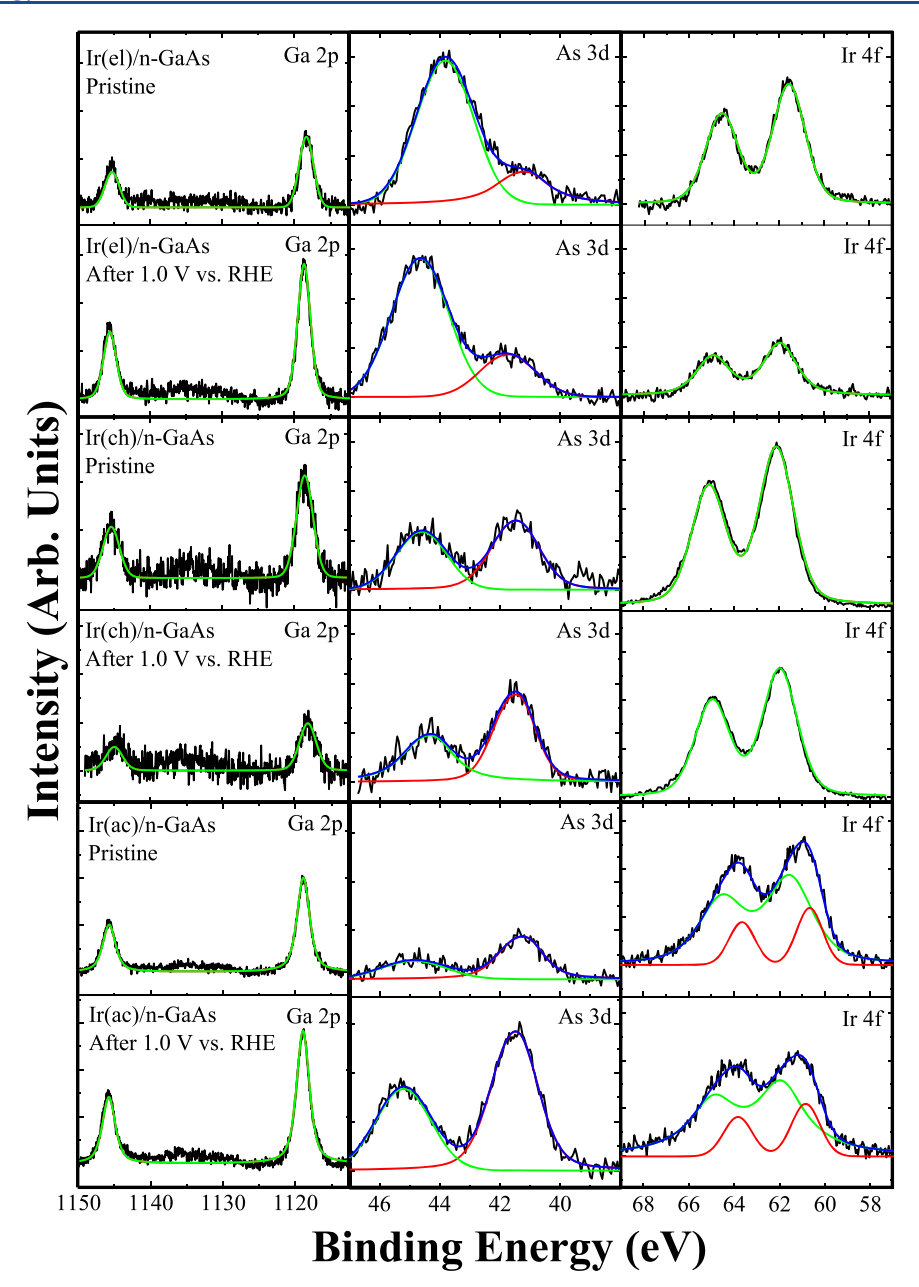


Figure 8. XPS spectra of Ir-coated n-GaAs ( $N_{\rm D}\approx 10^{18}~{\rm cm}^{-3}$ ) photoanodes. Samples are (top two rows) 24 h electroless iridium (Ir(el)), (middle two rows) spin-coated iridium acetylacetonate (Ir(ac)) coated n-GaAs. For each Ir type, the top row is pristine as-deposited and the bottom row is after 2 h under 1 Sun at 1.0 V vs RHE in 1 M H<sub>2</sub>SO<sub>4</sub>. The binding energy ranges are for the (left column) Ga 2p, (middle column) As 3d, and (right column) Ir 4f regions.

remains possible leading to the fairly uniform distribution of small etch pits seen after 10 min of operation. After 2 h under illumination at 1.0 V vs RHE, the etch pits became deeper, undercutting the Ir surface layer and growing into each other. Despite the highly roughened surface of Ir(el)/n-GaAs after 2 h (Figure S8), the XPS still shows significant although decreased Ir 4f peaks corresponding to  $IrO_2$ . The presence of  $IrO_2$  after 2 h indicates that some areas of the surface were well-protected and had not yet been removed by undercutting.

An additional experiment was performed to investigate the possibility of using in situ electroless Ir deposition as an ongoing surface repair mechanism, allowing the cocatalyst to redeposit during operation and perhaps protect the surface in the etch pits. In this experiment, a normally prepared Ir(el)/n-GaAs photoanode in 1 mM H<sub>2</sub>IrCl<sub>6</sub>, 1 M H<sub>2</sub>SO<sub>4</sub> was cycled for

10 min between 10 s at 1.0 V vs RHE under 1 Sun followed by 10 s at the open-circuit voltage (OCV) in the dark (Figure S10). The iridium deposition bath as electrolyte was too strongly light-absorbing to utilize in situ UV—vis characterization, but ICP—MS measurements of the dissolved semiconductor elements indicated that the corrosion faradaic efficiency remained high (>90% at 10 min). Thus, whether the Ir(el) layer is too porous to be sufficiently protective, or the electroless deposition was too slow to be beneficial on the 10 s pulse time scale, or the galvanic displacement mechanism itself contributes too much surface corrosion, it was clear the thin Ir(el) layer did not provide sufficient stabilization to the n-GaAs surface to enable durable photoanodic water oxidation in acidic media.

For the spin-coated Ir layers on GaAs, XPS results showed differences in the interfacial chemical state as well (Figure 8). Ir(ch)/n-GaAs had significant As<sub>2</sub>O<sub>3</sub> present on the pristine surfaces. Although not as dominant as for the Ir(el) samples, the As 3d As<sub>2</sub>O<sub>3</sub> peak for Ir(ch) was more intense relative to the GaAs peak than observed for bare n-GaAs (Figure 5). This was attributed to surface oxidation during the catalyst annealing step to make IrO<sub>2</sub>. The Ir 4f peaks for Ir(ch)/n-GaAs were entirely assigned to IrO2 and were much more intense than the corresponding peaks for Ir(el)/n-GaAs owing to the more compact Ir film that resulted from spin-coating. Although a slight decrease in IrO2 peak intensity was observed after 2 h at 1.0 V vs RHE, the signal remained strong, which indicates that much of the surface was protected from corrosion. Instead, the charge passed by photogenerated holes was primarily directed through isolated pinholes in the Ir(ch) to form larger and fewer etch pits (Figure 7b). The Ir(ac) film, in contrast, did not display as much As<sub>2</sub>O<sub>3</sub> on the pristine surface (Figure 8). The Ir 4f peaks were also present at lower binding energy than the other Ir films and were deconvoluted and assigned to a combination of IrO2 and Ir. This XPS result of incomplete oxidation of the  $IrO_x$  film may explain why the SEM of the Ir(ac) layer shows a morphology which is less compact and more fluid than the Ir(ch) layer (Figure 7). Incomplete oxidation of the layer during the anneal step could also have prevented greater oxidation of the underlying GaAs surface, accounting for the decreased As<sub>2</sub>O<sub>3</sub> in the pristine state. After 2 h of operation at 1.0 V vs RHE, the Ir(ac)/n-GaAs Ir 4f peak intensities were almost unchanged, indicating much of the surface was still covered with the Ir(ac) layer. However, the As 3d As<sub>2</sub>O<sub>3</sub> peak after operation did significantly increase, which confirms that surface corrosion occurred to an appreciable extent.

# 4. CONCLUSIONS

Some III-V semiconductor materials, with excellent light absorption and charge-collection properties and tunable bandgaps via alloying, are among the most promising candidates for high efficiency photoanodes for photoelectrochemical energy-conversion and water-splitting. GaAs is one of the most well-developed and efficient III-V semiconductors, but it is notoriously unstable under photoelectrochemical oxidative conditions. The photocorrosion mechanism is complex and depends on the pH, crystal orientation, band energetics, and the doping. As seen herein, a slight increase in the n-GaAs doping density led to dramatically different current density vs potential behavior, with  $N_{\rm D} \approx 10^{18}$ cm<sup>-3</sup> doped material displaying the beginnings of degenerate behavior which enabled charges to tunnel through the band bending energy barrier and pass significant current to corrosion even in the dark. Moreover, quantification of Ga and As atoms in solution to determine the corrosion faradaic efficiency showed a change in the dissolution pathway at the higher potential.

To stabilize the n-GaAs surface under photoanodic operation, water oxidation should be kinetically promoted relative to corrosion and/or the Ga and As interface states should be prevented from directly interacting with and exchanging charge with the electrolyte. Three types of OER cocatalyst Ir layers were tested in this work to investigate their effect on the GaAs photocorrosion. As determined by in situ UV—vis spectroscopy, each Ir thin layer modestly decreased the corrosion faradaic efficiency over the first 15 min. After

that, enough surface area was covered with etch pits to provide a preferential pathway to direct charge to the corrosion reaction. Self-limiting surface coverage with electroless deposition of Ir provided a thin uniform layer, but the nature of the galvanic displacement process left the GaAs vulnerable to electrochemical attack. Compact Ir layers produced by spincoating and annealing Ir precursors more effectively protected a greater area of the surface, but rapid etching via pinholes in the catalyst film still eventually led to most of the charge being directed to corrosion. Thus, stabilizing this type of III-V semiconductor under relevant solar water-splitting conditions is an exceptionally difficult materials challenge. Even a single pinhole can result in a corrosion nucleation site which will grow and degrade the protection layer. Thicker catalyst layers may help to minimize pinholes, but such metal layers can lead to Fermi-level pinning and impede the photoelectrochemical junction. Using a buried p-n semiconductor junction to control the band bending, the photovoltage can be maintained despite a thick catalyst surface layer, but parasitic light absorption in the film is an issue. Thus, a pinhole-free, compact thin film is still desirable. Graphene is an ideal material for such a layer which has been shown to add durability to GaAs photoelectrodes, but it still degrades rapidly in aqueous media. 16 ALD protective coatings of inert materials with favorable interfacial charge-transfer properties have had the most success, but pinholes remain problematic. 15 Therefore, despite the difficulty many laboratories have had synthesizing and reproducing thick pinhole-free ALD layers of "leaky" TiO<sub>2</sub>, <sup>14,25</sup> this strategy currently remains the state-of-the-art for the protection of III-V photoanodes like GaAs.

#### ASSOCIATED CONTENT

# Supporting Information

The Supporting Information is available free of charge at https://pubs.acs.org/doi/10.1021/acsaem.1c01768.

Additional data on photoelectrochemical behavior of bare n-GaAs, in situ UV—vis spectroscopy control measurements, in situ UV—vis spectroscopy calibration data, bare n-GaAs corrosion SEM images, Ir(el)/n-GaAs EDS map, spin-coated Ir layer transmittance vs thickness data, photoelectrochemical behavior of Ir(ac)/n-GaAs with Ir layer thickness, Ir/n-GaAs corrosion SEM images, and current density vs time for in situ electroless deposition of Ir (PDF)

# AUTHOR INFORMATION

#### **Corresponding Author**

Joshua M. Spurgeon — Conn Center for Renewable Energy Research, University of Louisville, Louisville, Kentucky 40292, United States; orcid.org/0000-0002-2987-0865; Email: joshua.spurgeon@louisville.edu

#### **Authors**

Sahar Pishgar — Conn Center for Renewable Energy Research and Department of Physics and Astronomy, University of Louisville, Louisville, Kentucky 40292, United States;
ocid.org/0000-0002-7754-5362

Matthew C. Mulvehill – Conn Center for Renewable Energy Research, University of Louisville, Louisville, Kentucky 40292, United States

- Saumya Gulati Conn Center for Renewable Energy Research, University of Louisville, Louisville, Kentucky 40292, United States
- Gamini U. Sumanasekera Conn Center for Renewable Energy Research and Department of Physics and Astronomy, University of Louisville, Louisville, Kentucky 40292, United States

Complete contact information is available at: https://pubs.acs.org/10.1021/acsaem.1c01768

# **Author Contributions**

The manuscript was written through contributions of all authors. All authors have given approval to the final version of the manuscript.

#### **Funding**

This material is based in part upon work supported by the National Science Foundation under Grant No. 1943977.

#### **Notes**

The authors declare no competing financial interest.

# ACKNOWLEDGMENTS

The authors acknowledge support from the Conn Center for Renewable Energy Research at the University of Louisville. This material is based in part upon work supported by the National Science Foundation under Grant No. 1943977.

#### REFERENCES

- (1) Lewis, N. S.; Nocera, D. G. Powering the planet: Chemical challenges in solar energy utilization. *Proc. Natl. Acad. Sci. U. S. A.* **2006**, *103* (43), 15729–15735.
- (2) Walter, M. G.; Warren, E. L.; McKone, J. R.; Boettcher, S. W.; Mi, Q. X.; Santori, E. A.; Lewis, N. S. Solar Water Splitting Cells. *Chem. Rev.* **2010**, *110* (11), 6446–6473.
- (3) Hu, S.; Xiang, C. X.; Haussener, S.; Berger, A. D.; Lewis, N. S. An analysis of the optimal band gaps of light absorbers in integrated tandem photoelectrochemical water-splitting systems. *Energy Environ. Sci.* **2013**, *6* (10), 2984–2993.
- (4) Zhou, X. H.; Liu, R.; Sun, K.; Friedrich, D.; McDowell, M. T.; Yang, F.; Omelchenko, S. T.; Saadi, F. H.; Nielander, A. C.; Yalamanchili, S.; Papadantonakis, K. M.; Brunschwig, B. S.; Lewis, N. S. Interface engineering of the photoelectrochemical performance of Ni-oxide-coated n-Si photoanodes by atomic-layer deposition of ultrathin films of cobalt oxide. *Energy Environ. Sci.* 2015, 8 (9), 2644–2649.
- (5) Zhao, J. H.; Gill, T. M.; Zheng, X. L. Enabling silicon photoanodes for efficient solar water splitting by electroless-deposited nickel. *Nano Res.* **2018**, *11* (6), 3499–3508.
- (6) Kim, T. W.; Choi, K. S. Nanoporous BiVO4 Photoanodes with Dual-Layer Oxygen Evolution Catalysts for Solar Water Splitting. *Science* **2014**, 343 (6174), 990–994.
- (7) Shi, X. J.; Choi, Y.; Zhang, K.; Kwon, J.; Kim, D. Y.; Lee, J. K.; Oh, S. H.; Kim, J. K.; Park, J. H. Efficient photoelectrochemical hydrogen production from bismuth vanadate-decorated tungsten trioxide helix nanostructures. *Nat. Commun.* **2014**, *5*, 4775.
- (8) Alqahtani, M.; Ben-Jabar, S.; Ebaid, M.; Sathasivam, S.; Jurczak, P.; Xia, X.; Alromaeh, A.; Blackman, C.; Qin, Y.; Zhang, B.; Ooi, B. S.; Liu, H.; Parkin, P.; Wu, J. Gallium Phosphide photoanode coated with TiO<sub>2</sub> and CoO<sub>x</sub> for stable photoelectrochemical water oxidation. *Opt. Express* **2019**, *27* (8), A364–A371.
- (9) Verlage, E.; Hu, S.; Liu, R.; Jones, R. J. R.; Sun, K.; Xiang, C. X.; Lewis, N. S.; Atwater, H. A. A monolithically integrated, intrinsically safe, 10% efficient, solar-driven water-splitting system based on active, stable earth-abundant electrocatalysts in conjunction with tandem III-V light absorbers protected by amorphous TiO2 films. *Energy Environ. Sci.* 2015, 8 (11), 3166–3172.

- (10) van de Krol, R.; Gratzel, M. Photoelectrochemical Hydrogen Production; Springer: New York, 2014.
- (11) Young, J. L.; Steiner, M. A.; Doscher, H.; France, R. M.; Turner, J. A.; Deutsch, T. G. Direct solar-to-hydrogen conversion via inverted metamorphic multi-junction semiconductor architectures. *Nature Energy* **2017**, *2* (4), 17028.
- (12) Chen, S. Y.; Wang, L. W. Thermodynamic Oxidation and Reduction Potentials of Photocatalytic Semiconductors in Aqueous Solution. *Chem. Mater.* **2012**, *24* (18), 3659–3666.
- (13) Pourbaix, M. Atlas of Electrochemical Equilibria in Aqueous Solution. Pergamon Press: Oxford, 1966.
- (14) Hu, S.; Shaner, M. R.; Beardslee, J. A.; Lichterman, M.; Brunschwig, B. S.; Lewis, N. S. Amorphous TiO2 coatings stabilize Si, GaAs, and GaP photoanodes for efficient water oxidation. *Science* **2014**, *344* (6187), 1005–1009.
- (15) Liu, R.; Zheng, Z.; Spurgeon, J.; Yang, X. Enhanced photoelectrochemical water-splitting performance of semiconductors by surface passivation layers. *Energy Environ. Sci.* **2014**, *7* (8), 2504–2517.
- (16) Yang, F.; Nielander, A. C.; Grimm, R. L.; Lewis, N. S. Photoelectrochemical Behavior of n-Type GaAs(100) Electrodes Coated by a Single Layer of Graphene. *J. Phys. Chem. C* **2016**, *120* (13), 6989–6995.
- (17) Hu, S.; Lewis, N. S.; Ager, J. W.; Yang, J. H.; McKone, J. R.; Strandwitz, N. C. Thin-Film Materials for the Protection of Semiconducting Photoelectrodes in Solar-Fuel Generators. *J. Phys. Chem. C* **2015**, *119* (43), 24201–24228.
- (18) Ben-Naim, M.; Palm, D. W.; Strickler, A. L.; Nielander, A. C.; Sanchez, J.; King, L. A.; Higgins, D. C.; Jaramillo, T. F. A Spin Coating Method To Deposit Iridium-Based Catalysts onto Silicon for Water Oxidation Photoanodes. ACS Appl. Mater. Interfaces 2020, 12 (5), 5901–5908.
- (19) Jiang, C. R.; Wu, J.; Moniz, S. J. A.; Guo, D. Q.; Tang, M. C.; Jiang, Q.; Chen, S. M.; Liu, H. Y.; Wang, A. Q.; Zhang, T.; Tang, J. W. Stabilization of GaAs photoanodes by in situ deposition of nickelborate surface catalysts as hole trapping sites. *Sustain. Energy Fuels* **2019**, 3 (3), 814–822.
- (20) Allongue, P.; Souteyrand, E.; Allemand, L. Charge-transfer Process at Illuminated Semiconductor Electrolyte Junctions Modified by Electrodeposition of Microscopic Metal Grain. *J. Electrochem. Soc.* 1989, 136 (4), 1027–1033.
- (21) Frese, K. W.; Madou, M. J.; Morrison, S. R. Investigation of Photoelectrochemical Corrosion of Semiconductors. 3. Effects of Metal Layer on Stability of GaAs. *J. Electrochem. Soc.* **1981**, 128 (9), 1939–1943.
- (22) Madou, M. J.; Frese, K. W.; Morrison, S. R. Influence of Surface Damage on Stabilization Against Photo-decomposition of n-type GaAs. J. Electrochem. Soc. 1980, 127 (4), 987–989.
- (23) Menezes, S.; Heller, A.; Miller, B. Metal Filmed Semiconductor Photoelectrochemical Cells. *J. Electrochem. Soc.* **1980**, *127* (6), 1268–1273.
- (24) Noufi, R.; Tench, D.; Warren, L. F. Protection of n-GaAs Photoanodes with Photoelectrochemically Generated Polypyrrole Films. *J. Electrochem. Soc.* **1980**, 127 (10), 2310–2311.
- (25) Shen, X.; Yao, M. Q.; Sun, K.; Zhao, T. S.; He, Y. L.; Chi, C. Y.; Zhou, C. W.; Dapkus, P. D.; Lewis, N. S.; Hu, S. Defect-Tolerant TiO2-Coated and Discretized Photoanodes for > 600 h of Stable Photoelectrochemical Water Oxidation. *Acs Energy Letters* **2021**, 6 (1), 193–200.
- (26) Allongue, P.; Blonkowski, S. Corrosion of III-V Compounds A Comparative Study of GaAs and InP. 2. Reaction Scheme and Influence of Surface Properties. *J. Electroanal. Chem. Interfacial Electrochem.* 1991, 317 (1–2), 77–99.
- (27) Khader, M. M.; Hannout, M. M.; Eldessouki, M. S. Photoelectrochemical Dissociation of Water at Silicon Doped n-GaAs Electrodes. *Int. J. Hydrogen Energy* **1991**, *16* (12), 797–803.
- (28) Lai, J. H.; Yuan, D.; Huang, P.; Zhang, J.; Su, J. J.; Tian, Z. W.; Zhan, D. P. Kinetic Investigation on the Photoetching Reaction of n-

- Type GaAs by Scanning Electrochemical Microscopy. *J. Phys. Chem. C* **2016**, *120* (30), 16446–16452.
- (29) Sharma, H.; Moumanis, K.; Dubowski, J. J. pH-Dependent Photocorrosion of GaAs/AIGaAs Quantum Well Microstructures. *J. Phys. Chem. C* **2016**, *120* (45), 26129–26137.
- (30) Nezhad, M. R. H.; Aizawa, M.; Porter, L. A.; Ribbe, A. E.; Buriak, J. M. Synthesis and patterning of gold nanostructures on InP and GaAs via galvanic displacement. *Small* **2005**, *1* (11), 1076–1081.
- (31) Pham, N. D.; Park, S. J.; Lee, J. P.; Oh, I. Galvanic Displacement of Gallium Arsenide Surface: A Simple and Low-Cost Method to Deposit Metal Nanoparticles and Films. *J. Chem.* **2014**, 2014, 1–8.
- (32) Sayed, S. Y.; Daly, B.; Buriak, J. M. Characterization of the interface of gold and silver nanostructures on InP and GaAs synthesized via galvanic displacement. *J. Phys. Chem. C* **2008**, *112* (32), 12291–12298.
- (33) Buabthong, P.; Ifkovits, Z. P.; Kempler, P. A.; Chen, Y. K.; Nunez, P. D.; Brunschwig, B. S.; Papadantonakis, K. M.; Lewis, N. S. Failure modes of protection layers produced by atomic layer deposition of amorphous TiO2 on GaAs anodes. *Energy Environ. Sci.* **2020**, *13* (11), 4269–4279.
- (34) McCrory, C. C. L.; Jung, S.; Ferrer, I. M.; Chatman, S. M.; Peters, J. C.; Jaramillo, T. F. Benchmarking Hydrogen Evolving Reaction and Oxygen Evolving Reaction Electrocatalysts for Solar Water Splitting Devices. *J. Am. Chem. Soc.* **2015**, *137* (13), 4347–4357.
- (35) Papaderakis, A.; Mintsouli, I.; Georgieva, J.; Sotiropoulos, S. Electrocatalysts Prepared by Galvanic Replacement. *Catalysts* **2017**, *7* (3), 80.
- (36) Pishgar, S.; Strain, J. M.; Gulati, S.; Sumanasekera, G.; Gupta, G.; Spurgeon, J. M. Investigation of the photocorrosion of n-GaP photoanodes in acid with in situ UV-Vis spectroscopy. *J. Mater. Chem. A* **2019**, *7* (44), 25377–25388.
- (37) Spurgeon, J. M.; Velazquez, J. M.; McDowell, M. T. Improving O<sub>2</sub> Production of WO<sub>3</sub> Photoanodes with IrO<sub>2</sub> in Acidic Aqueous Electrolyte. *Phys. Chem. Chem. Phys.* **2014**, *16* (8), 3623–3631.
- (38) Schlesinger, T. E. Gallium Arsenide. In *Encyclopedia of Materials: Science and Technology*; Elsevier Ltd.: Amsterdam, 2001; pp 3431–3435.
- (39) Allongue, P.; Blonkowski, S. Corrosion of III-V Compounds A Comparative Study of GaAs and InP. 1. Electrochemical Characterization Based on Tafel Plot Measurements. *J. Electroanal. Chem. Interfacial Electrochem.* 1991, 316 (1–2), 57–77.
- (40) Allongue, P.; Blonkowski, S. Influence of the Doping Concentration on the Electrochemical Etching of Semiconductors. *Electrochim. Acta* **1993**, 38 (7), 889–895.
- (41) Schroder, K.; Memming, R. Analysis of Trapping and Recombination Effects in Photoelectrochemical Processes at Semiconductor Electrodes Investigations at n-GaAs. *Berichte Der Bunsen-Gesellschaft-Physical Chemistry Chemical Physics* 1985, 89 (4), 385–302
- (42) Solomun, T.; McIntyre, R.; Richtering, W.; Gerischer, H. Surface Stoichiometric Changes of n-GaAs after Anodic Treatment An XPS Study. Surf. Sci. 1986, 169 (2–3), 414–424.
- (43) Huang, Y.; Luo, J. L.; Ivey, D. G. Comparative study of GaAs corrosion in H2SO4 and NH3 center dot H2O solutions by electrochemical methods and surface analysis. *Mater. Chem. Phys.* **2005**, 93 (2–3), 429–442.
- (44) King, D. E.; Fernandez, J. E.; Swartz, W. E. An XPS Study of the Doping of Trans, Trans-para-distyrylbenzene with AsF5 A Model Conducting Polymer System. *Appl. Surf. Sci.* **1990**, 45 (4), 325–339.
- (45) Contour, J. P.; Massies, J.; Saletes, A. X-ray Photoelectron Spectroscopy Study of GaAs (001) and InP (001) Cleaning Procedures Prior to Molecular Beam Epitaxy. *Japanese Journal of Applied Physics Part 2-Letters* 1985, 24 (7), L563–L565.
- (46) Ellis, A. B.; Bolts, J. M.; Kaiser, S. W.; Wrighton, M. S. Study of n-type Gallium Arsenide-based and Gallium Phosphide-based Photoelectrochemical Cells Stabilization by Kinetic Control and

- Conversion of Optical Energy to Electricity. J. Am. Chem. Soc. 1977, 99 (9), 2848–2854.
- (47) Kohl, P. A.; Wolowodiuk, C.; Ostermayer, F. W. The Photoelectrochemical Oxidation of (100), (111), and (111) n-InP and n-GaAs. *J. Electrochem. Soc.* **1983**, *130* (11), 2288–2293.
- (48) Djokic, S. S. Fundamentals of Electroless Deposition. In *Encyclopedia of Interfacial Chemistry*; Wandelt, K., Ed.; Elsevier: Amsterdam, 2018; pp 161–173.